NASA TECHNICAL MEMORANDUM

NASA TM X-68152

NASA TM X-68152

USE OF LEED, AUGER EMISSION SPECTROSCOPY AND FIELD ION MICROSCOPY IN MICROSTRUCTURAL STUDIES

by John Ferrante, Donald H. Buckley,
Stephen V. Pepper and William A. Brainard
Lewis Research Center
Cleveland, Ohio

TECHNICAL PAPER presented at the
Tools and Techniques for Microstructural Analysis Conference
sponsored jointly by the American Society for Metals
and the International Microstructural Analysis Society
Chicago, Illinois, September 17-18, 1972

СОЬА
CV2E LIFE

USE OF LEED, AUGER EMISSION SPECTROSCOPY AND FIELD ION MICROSCOPY IN MICROSTRUCTURAL STUDIES

by John Ferrante, Donald H. Buckley, Stephen V. Pepper and William A. Brainard

Lewis Research Center

E-7103

INTRODUCTION

The past fifteen years have produced great advances in the experimental study of solid surfaces. Vacuum systems that will readily attain pressures in the 10^{-11} to 10^{-10} torr range are commercially available. Thus, once a surface is cleaned, the researcher has adequate time to obtain information before a contaminant film can form. Accompanying these advances in obtaining low pressures in clean systems has been the development of analytic tools for examining surfaces such as LEED (low energy electron diffraction), AES (Auger emission spectroscopy), and FIM (field ion microscopy).

The objective of the present paper will be to present a brief description of these analytical tools and then to show how they have been used to study adsorption, friction, adhesion, and wear by Buckley and his co-workers at the NASA Lewis Research Center.

Friction and lubrication are subjects which are of wide practical interest. Their importance ranges from design of gears and bearings to bone transplants. In spite of the importance of the field, little emphasis has been placed upon a basic understanding of phenomena. For example, the physics of the short range interplanar attraction of two metallic surfaces is not fully understood.[1] Most of the basic studies,

which were pioneered by Bowden and Tabor,[2] have concentrated on mechanical properties of materials such as hardness, slip, yield strength, etc. The advent of ultra-high vacuum systems and surface diagnostic equipment enable greater control of environments and open new possibilities in examining the friction and lubrication process. It is now possible to concentrate on atomic and chemical effects in the friction process.

Basic to the friction process is adhesion[2, 3] i.e., the interplanar attraction between two surfaces. The quantity referred to as the friction force refers in general to the force necessary to break this interplanar bond in shear for sliding surfaces and in tension for rolling surfaces. The most dramatic form of failure with materials in contact is adhesive wear where, as a result of adhesion, particles are torn from one of the contacting surfaces leaving a greatly disrupted surface and a wear particle which can act as an abrasive. This interplanar adhesive force is altered markedly by types of material, surface films (such as oxides), and lubricants (both solid and fluid). LEED, AES, and FIM are ideal for such studies where the domain of interest is the top most atomic layers.

The purpose of these studies is to gain a fundamental understanding of adhesion and dynamic friction on an atomic or microscopic level and hopefully to later establish material properties based on these observations which will prove to be useful for design of practical equipment such as bearings.

BACKGROUND

Before describing experiments using LEED, AES, and FIM, a brief introductory background describing each technique will be presented. It

is hoped that although brief this background will be sufficient to supply the unfamiliar reader with enough information to understand the applications to the experiments which follow.

A. LEED

Electron diffraction[4] was experimentally demonstrated by Davison and Germer in 1927. Davison and Germer showed that as a result of the wave nature of an electron, the electrons could be diffracted by a crystal lattice in a manner similar to x-ray diffraction. Following this early work only H. E. Farnsworth at Brown University[5] pursued the technique as a surface analytical tool using a Faraday cup to detect the diffracted electrons. The reason that low energy electrons (0 to 200 eV) can be used to examine surfaces is that the penetration of these electrons should be limited to the first few atomic layers. LEED became a popular surface analytic tool in the late 1950's when L. H. Germer of the Davison-Germer experiment suggested that the diffraction pattern could be displayed on a fluoroscent screen by post-accelerating the diffracted electrons.

Figure 1 indicates simply the diffraction process in LEED if the crystal were a two-dimensional lattice. An electron gun shoots a beam of electrons of a given energy at the crystal. The electrons are diffracted by the lattice and the diffraction pattern is observed on the fluoroscent screen. Figure 2 shows the Ewald construction for a given energy (eV) and wavelength (λ) of the incident electrons. In LEED as in x-ray diffraction you are observing the reciprocal lattice. The reciprocal lattice for a two-dimensional array is a set of rods. It can be seen that for a two-dimensional mesh a diffraction spot should always appear; this is not the case, however, since three-dimensional effects in a real crystal modulate the diffracted beam intensity.

Figure 3 gives the typical structural arrangement in the post-accelerated LEED system. The first grid is grounded giving a field free region; the second grid (now generally two grids for better resolution in Auger work) repels all the scattered electrons but those at the primary beam energy (i.e., elastically scattered), and the final grid is grounded in order to shield the retarding grids from the high voltage on the fluorescent screen.

As example of a LEED pattern figure 4 shows the LEED pattern of a clean (110) tungsten surface. Note that the diffraction pattern has the characteristic symmetry of a bcc (110) surface in the direct lattice. The LEED pattern on the right is the pattern which results when what is thought to be 1/2 monolayer[6] of oxygen is adsorbed on the surface. Note the additional spots located at (1/2, 1/2) positions. In the direct lattice these represent rows of atoms with double the spacing of the substrate. Figure 5 shows the LEED pattern of the same surface contaminated with carbon. The interpretation of this pattern in the direct lattice is given in figure 6.[7] It can be seen that the complicated multispotted diffraction pattern represents a sparsely populated direct lattice structure. Some additional comments are necessary regarding the interpretation of LEED patterns. Since the pattern is in the reciprocal lattice you cannot unambiguously arrive at a direct lattice structure without examining spot intensitites as in x-ray diffraction. The interpretation of LEED patterns is presently a subject of intense study.[8] In some cases simple interpretations seem to be valid, in others they are not.

B. AES

Auger electron spectroscopy[9] was suggested as a tool for performing surface chemical analysis in 1953 by Lander. However, it did not become a popular surface analytical tool until the late 1960's when L. A. Harris[10] suggested that electronic techniques for extracting small signals from a large background be applied to Auger analysis.

In order to explain the application of AES, a comparison is made with photon emission spectroscopy in figure 7. The first step in the process is excitation of the atom to be detected. Then the radiation must be energy analyzed. The resulting spectrum must be detected and then analyzed for the species present. In figure 8[11] we describe the basic Auger process. First an inner level is ionized. An electron drops from an upper level and releases a fixed quantity of energy equal to the difference in energy of the two levels. This energy is absorbed by an electron in an upper level and if the energy of this electron is sufficient, it can escape from the solid. In general the higher the atomic number of the material, the more peaks available for analysis. However, the higher the atomic number, the lower the probability that an Auger electron will be emitted from the material as opposed to an x-ray. All elements except hydrogen can be detected with AES. AES is a surface sensitive tool since the energies of the electrons studied are sufficiently low that they can only originate from a few atomic layers. The sensitivity of AES is of the order of 0.01 monolayers.[11]

A typical energy distribution for secondary electrons emitted by a solid is shown in figure 9. The high energy peak consists of electrons

which are essentially elastically scattered and it is these electrons which are used in LEED. The peaks in the expanded scale arise from excitations resulting in fixed energy losses from the incident energy such as plasmons or interband transitions. The large low energy peak represents the true secondaries. The principle Auger peaks are located in the flat region. An Auger peak can be distinguished from other peaks by varying the incident electron energy. The Auger peak remains at the same energy since its position only depends on differences in energy between energy levels. Figure 10 shows an oxygen Auger peak extracted from the background using a background nulling techniques suggested by Musket and Ferrante.[12]

In general, however, extracting a peak from the background directly is difficult since the amplifier is overloaded before the peak can be resolved. This is where the technique suggested by Harris can most effectively be applied. By taking the derivative of this spectrum the relatively flat background can be eliminated and the peak, where large changes are occurring, can be extracted. Figure 11 gives an example of a derivative spectrum.

Two types of AES apparatus are generally in use.[11] The first which uses LEED optics is shown in figure 12. Either the LEED electron gun or a side gun are used to excite the Auger electrons. The LEED screen is used for detection. The center grids have a retarding voltage applied to them which sweeps through the entire energy spectrum. A small perturbing potential is superimposed on the retarding voltage at a known frequency. This retarding voltage enables differentiation of the signal using phase sensitive detection techniques. The perturbing signal is fed into the reference channel of a lock-in amplifier from the same oscillator to

permit phase matching. The first derivative is the coefficient of the fundamental frequency as detected by the lock-in amplifier and the second derivative is the coefficient of second harmonic. The first derivative of the detection current is the secondary electron distribution function shown in figure 9. Figure 13 gives an example of the differentiation scheme along with a Taylor expansion of the perturbed current. Figure 14 shows the results of this differentiation on peaks generally observed in AES. Figure 15 shows the latest form of Auger analyzer in use, the cylindrical mirror analyzer (CMA). With this analyzer only those electrons with an energy spread $\pm\Delta E$ about the retarding voltage are collected. Therefore the signal in this case corresponds to the derivative of the current in the LEED apparatus or the secondary electron energy distribution. The first derivative corresponds to the second derivative for LEED optics or the standard Auger spectrum. The CMA has a higher signal to noise ratio and sensitivity than the LEED, Auger analyzer. The improved signal to noise ratio reduces the need for output filtering and thus allows very fast sweep speeds (0.1 sec) and display on an oscilloscope. Its main disadvantages are its rather bulky size and the necessity of being close (0.5 cm) to the analyzed specimen.

C. FIELD ION MICROSCOPY

The field-ion microscope was invented by Professor Erwin Mueller[13] in 1951 many years after his development of the field emission microscope. Field ion microscopy is a technique for looking at the atomic structure of a surface directly with a resolution of 2.5 Å. It has proven to be a useful research tool for both metallurgists and surface physicists since its development in 1951.

Figure 16 gives a schematic of the field-ion microscope. A wire hemispherical tip approximately 500 Å in diameter is produced by electro-etching. In use the tip is biased to a high positive potential relative to a phosphor-coated screen. Once the vacuum system is evacuated, the system is filled with helium to pressures of 10^{-3} torr. The surface is cleaned by applying high positive electric fields of sufficient strength to tear atoms from the surface (field evaporation). This cleaning process also creates a near-perfect hemispherical surface by removing asperities and other imperfections from the surface. For the most part refractories have been studied with FIM since refractory tips are most easily formed and can withstand the high fields involved, however, iron, copper, nickel, cobalt, and gold have also been studied.

Figure 17 demonstrates the basic principle of operation of the FIM. A helium atom impinging on the tip experiences a very high electric field resulting from the curvature of the tip. This field polarizes the atom and distorts the atomic potential enough so that there is a reasonable probability that an electron will tunnel from the atom to the metal leaving behind a helium ion. The atom hops on the surface several times until it is accommodated at a distance sufficient for the tunneling to occur. If it gets too close (dashed line) the atomic energy level lies below the Fermi Energy leaving no states to tunnel to. This ionization occurs directly above atoms located in the tip where the field is highest. For the most part only 10 to 15 percent of the atoms on the tip located at the zone edges and at the kink sites are visible. These ions are then accelerated to a phosphorescent screen at a large distance from the tip giving the high magnification. The FIM gives much higher resolution than the field electron microscope

(2.5 Å as compared to 25 Å), since the lateral uncertainty in position is much lower with ions and the thermal part of this uncertainty in position can be lowered by cooling the tip to liquid hydrogen or liquid helium temperatures.

Figure 18 is a typical FIM pattern for a clean tungsten tip oriented in the (110) direction. The small rings are various crystallographic planes that would appear on the hemispherical surface. Figure 19 shows a stereographic projection of the tip indicating the plane locations.

A color superposition technique can be used to examine changes in the tip surface. With this technique the before and after black and white micrographs are photographed on the same color plate by superimposing one on the other. The before black and white micrograph is photographed with a green filter and the after with a red filter. Any spot which will photograph with both green and red will appear as yellow, a spot appearing only in the first micrograph will appear as green and a spot only appearing in the second as red. Thus green spots indicate the location of surface atoms which have been lost, red spots where new atoms appear, and yellow spots where there has been no change.

As with LEED the interpretation of field ion micrographs requires considerable care: An accurate interpretation requires knowledge of the geometry of the surface, the interaction of a defect with the surfaces, and the mechanism of image formation itself. In-depth discussions of the interpretation of field ion micrographs are available in the literature.[13]

A. Application of LEED, AES, and FIM to Friction, Adhesion and Wear

A schematic diagram of the LEED-AES-Adhesion apparatus is shown in figure 20.[14, 15] A single crystal or polycrystalline sample is mounted at the center of curvature of the LEED screen. The sample can be analyzed by LEED for crystal structure changes and by AES for chemical analysis of the surface region. It is also possible to ion-bombardment clean the crystal, heat the crystal, and to bleed in various contaminant gases. Once the crystal condition has been predetermined, it is rotated and adhesive contact is made with a cylindrical specimen approximately 2 to 4 mm in diameter mounted on the pivot arm shown in figure 21. The force necessary to break the adhesive bond is then determined by a calibrated magnetic drive system. The contacted surface can be analyzed for structural changes by LEED and chemical changes with AES.

The stainless steel vacuum system is bakable to 250°C. It is evacuated by roughing with sorption pumps. The final evacuation is accomplished with a titanium sublimation pump and a 140 l/s ion pump. The system has a base pressure in the 10^{-11} torr range and typically operates in the low 10^{-10} torr range as measured with a nude Baird-Alpert gage.

B. Pin and Disk AES Apparatus

A configuration widely used in the field of friction and wear is that of the pin on disk. An apparatus based on this configuration is shown in figure 21. The stainless steel vacuum chamber is evacuated first by cryosorption pumps and then by an ion pump. It is bakeable to 250°C and has a base pressure of 1×10^{-10} torr. A hemispherically tipped rider

contacts a flat disk mounted on a magnetic rotary feedthrough. The disk may be rotated and the friction force of the disk on the pin measured by a strain gage assembly connected through a bellows. Wear can be measured by removing the pin and disk and determining the amount of material removed from the pin, while the wear track can be studied with a surface profilometer.

The elements present in the wear track of the disk may be identified by a cylindrical mirror AES analyzer mounted to analyze a spot on the disk 153° away from the contact spot. This AES analyzer may be operated while the disk rotates and thus allows real-time monitoring of the surface chemistry of the wear track during sliding. The transfer of material from rider to disk, penetration of surface films and adsorbed gases are thus possible to detect. The disks may also be sputter cleaned by argon ion bombardment. This treatment removes the carbonacious and metal-oxide films normally present and produces atomically clean surfaces.

C. Field Ion Microscope - Adhesion Apparatus

The field ion microscope adhesion apparatus is shown in figure 22. The vacuum system associated with it is similar to those already mentioned.

The adhesion apparatus is a magnetically activated beam similar to that used in the LEED-AES adhesion experiments. However, this contacting system is considerably more sensitive than that in the LEED system due to the fragileness of the FIM tip. A Cahn microbalance with a sensitivity of 0.01 milligrams calibrates the loading system. Applied loads as low as 0.05 milligrams are possible. A photocell sensing system is used to determine beam position

and serves to damp out vibrations. The system is mounted on a vibration isolation table with a natural vibration of 1.1 hertz.

TYPICAL RESULTS OF STUDIES

A. LEED-AES Experiments

As was mentioned in the introduction, an understanding of adhesion is important to an understanding of friction. The LEED-AES experimental equipment shown in figure 20 has the capability of contributing to an understanding of adhesion. It enables characterization of the chemical composition of all surfaces and determination of the structure of single crystal surfaces before and after contact. Starting with a well characterized surface enables examining adhesive bonding forces and determining the effects of adsorbates on bonding.

An important result of these studies is that adhesion has occurred between all of a large number of clean metal surfaces,[14, 15] and, secondly, that transfer of material occurs from one surface to another. (Transfer of material is important since it indicates that the interfacial bonding can be stronger than self-bonding in one of the materials.) This was an unexpected result since there are some empirical theories of adhesion[16] that speculate that it should occur between mutually soluble metal combinations and that the strength of the bonding should be related to the solubility. Table I shows the results of adhesion studies performed between the (011) surface of iron and the densest packed planes of a number of other metals.[15] There is no correlation between the bonding force and solubility, whereas there is some correlation to cohesive energy and some correlation to chemical activity.

Figure 23 shows some results concerning the effect of adsorbates on adhesion. The upper curve shows the increase in breaking force with applied load, which is probably related to an increase in contact area. The lower curve shows the same system after a monolayer of oxygen has been adsorbed on the tantalum surface. There is a marked reduction in the binding force on the contaminated surface. An interesting further result of the studies is the fact that for the clean metal couples iron transferred to tantalum whereas for the oxidized tantalum surface oxygen transferred to iron. These results indicate on an atomic scale what effect lubricants have. The lubricant reduces the interfacial attraction between surfaces.

A number of studies are presently being carried out on adhesion with alloys. The object of these studies was to determine whether the chemical constitution of the alloy surface is the same as the bulk and if not to what extent does this departure from bulk constitution affect adhesion. Figure 24 shows the results of adhesion between a (111) gold surface and (111) pure copper, pure aluminum and alloys of aluminum in copper.[14] The adhesive force increased to that of pure aluminum with concentrations as low as 1 percent in the bulk. It was assumed that aluminum segregated at the surface of the alloy presenting essentially a pure aluminum interface. Subsequent AES studies[17, 18, 19] indicated that segregation of aluminum was occurring at the surface. As an example, figure 25 shows the increase in aluminum surface concentration following sputtering then annealing for a copper alloy containing 10 a/o aluminum. Combined LEED and AES studies indicated that aluminum atoms were on top of the alloy surface thus giving a surface layer that was entirely aluminum. It was speculated that equilibrium segregation of aluminum was occurring similar

to the process occurring at a grain boundary as described by McLean.[20] Figure 26[18, 19] shows the results of an Auger study on the copper 10% aluminum alloy in which the aluminum to copper Auger peak height ratio was examined as a function of temperature. The ratio was reversible with temperature indicating that equilibrium segregation of aluminum was occuring. The results of these studies suggest several possibilities for the friction and wear studies, namely it is possible that alloys could be fabricated with mechanical properties close to the solvent but frictional properties dominated by the solute. Another possibility arises concerning protective coatings. It has been observed[21] that oxides of solutes form on alloy surfaces. It is conceivable that surface segregation could be a contributing factor to the formation of these oxides. These oxides could provide corrosion resistance as well as altering the frictional behavior of the surface.

LEED represents an interesting tool for examining the effects of adhesion on the structure of single crystals. For example, it would be interesting to know if adhesion completely destroys the surface ordering after breaking the bond, if the order is maintained but some evidence of stress is observed, and if transfer has occurred does the transfer occur in an ordered or random manner. These structural considerations could shed some light on the nature of adhesion. Figures 27, 28, and 29[3, 15] give some example on the effects of adhesion on surface structure. Figure 27 shows the LEED patterns resulting from the contact of the (111) surface of the noble metals copper, silver and gold with iron (110) surface. It can be seen that the iron (110) structure remained the same, that additional spots appeared in the pattern, the additional spots

were the same for the three metals, and strain or some destruction of long range order occurred in a direction normal to the streaking shown in the patterns. It is tempting to attribute the additional spots observed to transfer of copper, silver, or gold to the iron surface in an ordered fashion. Figure 28[3] shows the results of contact of the most densely packed planes of copper, lead, and platinum to a nickel (111) surface. Again order is maintained in all cases, additional spots appear in the diffraction pattern for copper and lead, and no additional spots but surface strain appear after contact with platinum which does not transfer as indicated by AES. It is again tempting to assume that the additional spots represent transfer of material. Finally, figure 29 shows the results of contacting of oxidized tantalum and nickel to an iron (110) surface. Again additional spots appear on the iron surface with AES indicating that oxygen but no nickel or tantalum has transferred to the iron. Contacts with the clean tantalum and nickel pin gave no additional spots in the LEED pattern and showed no evidence of the transfer of nickel or tantalum to the iron.

The combination of LEED, AES, and adhesion can give much interesting information about the contact to two metal surfaces. Transfer, relative strength of bonding, effects of adsorption, effects of alloying and surface structure following fracture of the adhesive bond can be examined.

B. Pin and Disk Experiments

The main use of the pin and disk system with AES analyzer has been to examine transfer of materials in sliding contact. Figure 29 demonstrates transfer from an aluminum rider to a steel disk.[25] Both surfaces had their

normal oxide persent. Initially there is carbon present in the Auger spectrum, probably from carbon monoxide on the surface. After one pass of the rider over the disk an inflection occurs at the (70 eV) low energy aluminum peak. After twenty passes we see a distinct aluminum peak has grown out of the background and the carbon peak is reduced by being covered with aluminum. For a silver rider on a tungsten disk, a cyclic change in coverage occurs in which silver first coats the surface, is back-transferred and again coats the surface.[23]

The study of transfer has been investigated in more detail. NASA studies on the transfer mechanism have been made on dissimilar monocrystalline metals in simple touch contact.[3] These studies have led to a correlation for the direction of metal transfer when the adhesive junction is broken by simple tensile fracture. In all cases investigated, the cohesively weaker material transferred to the cohesively stronger. This indicates that the interfacial adhesive junction between the dissimilar metals is stronger than the cohesive bonds in the cohesively weaker of the two metals. Therefore, the critical physical property that determines the direction of transfer is the relative cohesive energy of the two materials. Since values of the cohesive energy of the elements are well known, a prediction of the direction of metallic transfer is easily obtained.

The metal transfer process for polycrystalline metals in sliding contact was examined to determine whether the above correlation for the direction of metallic transfer is valid for polycrystalline metals in sliding contact. The simple correlation was expected to require

modification, since the strengths of polycrystalline materials are functions of their grain structures and degree of work hardening. In addition, the interfacial adhesive junctions are fractured by shear stress, and not tensile stress.

Based on the cohesive-energy concepts, the disk and rider materials were chosen to transfer metal from rider to disk, where it could be detected by AES. Accordingly, the refractory metals, tungsten, tantalum, molybdenum, and niobium, were selected as disk materials. They all have high cohesive binding energies, with tungsten having the highest. The riders were iron, nickel, and cobalt. These metals have about the same cohesive energy,), and it is considerably lower than that of the refractory disks. Thus, transfer is expected from rider to disk in all cases.

The results for the 12 metal couples are presented in table II. Cobalt transferred to all four disks, while nickel and iron transferred only to tungsten.[23] If the relative cohesive energy determines the direction of transfer, then iron, nickel, and cobalt should all have transferred to the tungsten, tantalum, niobium, and molybdenum disks, since the former are cohesively weaker than the latter. Since they did not, relative cohesive energy alone does not provide a satisfactory guide to the direction of metallic transfer under conditions of sliding.

To understand the overall transfer results, the effect of crystal structure on the shear properties of materials must be considered. With sliding, the close-packed hexagonal metal, cobalt, develops a basal texture with basal planes parallel to the sliding interface.[24] This is the preferred slip plane and the easy shear plane in cobalt, and

the resistance to shear is minimal. Slip plane dislocations can easily move under the influence of the frictional shear force. With the limited number of slip systems operating in the hexagonal structure of cobalt, very little strain hardening occurs, and the easy shear property of the rider is maintained. The transfer of cobalt to the disks, therefore, proceeds as expected from simple adhesion concepts.

In contrast to cobalt, iron and nickel are cubic structures and will strain harden very readily because of the large number of slip systems operable in these metals and the corresponding concentration of slip system dislocations.[24] Sliding an iron or nickel rider on a disk will, therefore, result in considerable strain hardening of the rider in the vicinity of the contact.

Considering the cases of iron and nickel sliding on tantalum, niobium, and molybdenum, evidently the region most resistant to shear in the adhesive contact zone lies in the iron and nickel riders. This resistance to shear is a consequence of the strain hardening of the riders with sliding to the extent that they offer greater resistance to shear than do the disks. The rider strain hardens faster than does the disk because the rider is continually worked, whereas the disk is being worked along the entire circumference of the wear track. Shear, therefore, occurs in the tantalum, the niobium, and the molybdenum, and some of the molybdenum is transferred to the rider, as verified by AES analysis of the rider for the case of the nickel/molybdenum specimens.

On the other hand, for iron and nickel sliding on tungsten, the disk material with the greatest resistance to shear, an intermediate situation obtains. It was found that transfer occurred from the disk to the rider

(as verified by AES analysis of the rider for the case of Fe/W). This transfer in both directions indicates that the shear strengths of the work-hardened rider and wear track of the disk were about the same.

Therefore, while the cohesive energies of iron, nickel, and cobalt are similar, the strain-hardening characteristics of the metals undergoing sliding are different. The consequence of this difference is the failure of relative cohesive energy alone to provide a satisfactory guide to metallic transfer in this geometrically asymmetrical situation.

Another application of the pin and disk configuration is the study of polytetrafluoroethylene (PTFE) on various metals.[25] Because of its low friction and wear characteristics, it has found application in bearing surfaces with metal parts while its chemical inertness has made it attractive for corrosive media. In order to understand the low friction as well as the adhesion (or lack of it) knowledge of the PTFE metal interface is necessary.

In these experiments the adhesion, friction and transfer of PTFE to various metals was studied. The objective was to assess the effect of chemical constitution of the mating surfaces and ambient environment on the adhesion and friction of PTFE. The metal surfaces were both clean and oxidized as determined by AES.

To investigate the adhesion of PTFE to metals, the pin and disk apparatus was used in a static mode. Pins of PTFE were pressed onto the stationary disk in ultra-high vacuum by the deadweight loading system. After termination of this static contact the disk was rotated to bring the contact spot under the electron beam for AES analysis. Adhesion

between the PTFE and disk was deduced by the detection of PTFE (by AES) on the disk after the contact.

The results of the static contacts were that the transfer, and thus adhesion of the PTFE to the disks was independent of the chemical constitution of the surface of the disk. The disks surfaces were aluminum, iron, nickel, copper, silver, gold, tungsten, tantalum and aluminum oxide. All the experiments were performed on surfaces that were atomically clean.

The independence of the observed transfer on the chemical activity of the surfaces leads one to believe that the polymer is detached from the pin by general physical or van der Waals forces between the metal and the rider.

The adhesion of PTFE films to a substrate and the friction of PTFE are usually considered as separate problems. However, Makinson and Tabor[26] have proposed a model for the friction of PTFE that employs adhesion of PTFE as one of its components. The other component is that tangential motion of the contact results in the drawing out of lamellae of polymer from the body of the rider. The friction force thus results from the force necessary to draw these lamellae out and is not due to the traditional one of fracture in shear of adhesive junctions between the contacting bodies.

Evidence for the adhesion necessary to anchor the lamellae, has up to now received only circumstantial support. Makinson and Tabor considered the adhesion "very strong" whereas Steijn noted that it needs to be only strong enough to permit the drawing of lamellae to proceed. Here it has been shown that there is strong enough adhesion initiated by mechanical

static contact to allow fracture in the PTFE. This adhesion would then be strong enough to anchor the lamellae.

The adhesive transfer observed by static contact is independent of the chemical constitution of the substrate. The friction should then be independent of the environmental and chemical constitution of the substrate. The sliding experiments performed in this apparatus have confirmed that the low speed friction of PTFE is, in fact, independent of the chemical constitution of the substrate. Thus, an important aspect of the lamellae-drawing model of the friction of PTFE has been confirmed.

Information on the structure of the film and its interaction with the substrate may be obtained from the time dependence of the Auger peaks when the disk is stationary and the electron beam impinges on one spot of the surface. In figure 31 two spectra are exhibited, taken 60 seconds apart. It is seen that the fluorine peak has decreased while the carbon and tungsten peaks have grown. The incident 2000 eV electrons have severed the carbon-fluorine bonds in the PTFE and the fluorine has desorbed from the surface. The carbon remains behind on the surface. With the departure of the fluorine, Auger electrons from the carbon and tungsten beneath the fluorine can leave the surface and enter the analyzer, resulting in growth of these peaks. Exposure of the surface to the electron beam for about one minute resulted in complete disappearance of the fluorine peak.

However, surface species chemisorbed on metals are not subject to such rapid electron-induced desorption. It has been proposed that the slow desorption rate is due to the reformation of the bond initially broken by the bombarding electrons by tunneling of electrons from the

metal to the excited atom before it can leave the surface.[25] Such tunneling occurs only if the surface species is in intimate electronic contact with the metal, e.g., chemically bonded to it. The high desorption rate observed here thus indicates that there is no chemical bonding between the fluorine in the film and the metal substrate.

In contrast to the desorption of fluorine by the electron beam, the carbon remains on the surface. This behavior is consistent with the polymeric structure of PTFE, which is depicted in figure 32. While there is one chemical bond between fluorine and the carbon, the carbon atoms have four bonds, two with other carbons and two with fluorine. Since the two bonds retaining the carbon in the chain must both be broken for it to be desorbed, such desorption is a highly unlikely event with the electron beam current densities employed here. It thus appears from observations with AES that the transfer film is indeed a polymeric chain and that the fluorine in the film has no chemical interaction with the metal.

The simple observation of transfer and electron desorption in AES experiments has provided valuable information about interfacial bonding on both metals and insulators. These results emphasize the power of AES as a surface analytical tool.

C. Examples of Field Ion Microscope Results

A second method being used in our laboratory for studying adhesion is Field Ion Microscopy. FIM has the advantages that one can view the direct lattice rather than the reciprocal lattice as in LEED and it is possible to estimate binding energies of the transferred layer by the electric field required to desorb and the amount of subsurface damage from the number of layers stripped from the tip. In a sense an adhesion experiment performed with a field ion tip is analogous to a contact with

a single asperity. Again in FIM-adhesion experiments it is of interest to know whether transfer occurs in an ordered or disordered fashion. The study of adhesion using field ion microscopy was pioneered by E. Mueller in association with Nishikawa. [27] Most of their contacts were made in air and then put in the system and imaged. This paper will not present their work. In this paper the results of experiments performed by Brainard and Buckley[28] will be presented. In these experiments all adhesive contacts were made in the vacuum system. The work will discuss studies performed concerning gold and platinum in contact with a tungsten tip [28] and the contact of PTFE with a tungsten tip.[29]

Figure 18 shows the FIM pattern from a clean tungsten tip following cleaning oriented with the (110) direction parallel to the axis of the tip. Figure 19 shows a sterographic projection of the tip. Figure 33 shows the same tip following contact with platinum imated at 14 kV. There are several observations that can be immediately made. First, there is considerable disorder characterized by many random bright spots. Second, the character of several planes has changed. For example, on (211) the inner ring has decreased in diameter and is considerably disordered on the plane edge. The (111) plane shows deviation from normal packing and the higher index planes are completely obscured. It is believed that micrographs after contact show a platinum layer that is partially ordered after tungsten contact with changes that represent the transition from an ordered tungsten to a platinum surface.

Contact of the tip with gold was also examined. Figure 34 shows the results of this contact. The only ordering evident is on the (110) planes which are believed to be underlying tungsten atoms. Figure 35 shows the same tip with the imaging voltage increased. It can be seen that diffuse spots begin to appear. Further, field evaporation caused by the increased imaging voltage (fig. 34) results in

the appearance of clusters on the tip surface. These patterns represent a situation where the gold transfers to the tungsten with no crystallinity, rather it is fairly randomly distributed with some apparent clustering of the gold atoms. Similar results were obtained with an iridium tip oriented with its axis parallel to the (001) direction.

The above results seem to agree with vapor deposition studies performed on tungsten tips although the conditions are radically different. In the adhesion experiments platinum was ordered after contact gold was not. Vapor deposited films of platinum on tungsten[30] showed a high degree of order at 118 K. Whereas for gold deposited on tungsten at 78 K[31] it was necessary to heat to 800 K before ordering occurred. It cannot be absolutely concluded at present that the changes observed are deposited films although it is highly plausible. Future inclusion of the atom probe in these experiments will settle this point.

As a final example of the FIM studies the results of contacts made with PTFE to a tungsten tip oriented in the (110) direction are shown. Figure 36 represents the results of contacting the tungsten with PTFE. It can be seen that some of the spots are suggestive of the end view of a PTFE chain shown on the bottom of the figure.

The bonding is strong enough to withstand the helium image field without desorption suggestive of chemisorption of PTFE to the tungsten. Figure 37 shows the results of applying a heavy load to the tungsten tip with PTFE. We see the surprising result that extensive deformation of the tungsten occurred. This pattern was taken after the PTFE was desorbed. The deformation probably is not the result of bending the shank of the tip since the (110) plane is in the same position on the FIM screen.

FIM complements other surface analytic tools in the study of contact between solid surfaces. It can provide information concerning ordering, strength of bonding and transfer. FIM has the advantage that structural changes can be observed in the direct lattice.

Concluding Remarks

Surface research tools such as LEED (low energy electron diffraction), Auger emission spectroscopy analysis, and field ion microscopy have been discussed. Examples of their use in studying adhesion, friction, wear, and lubrication have been presented. These tools have provided considerable insight into the basic nature of solid surface interactions.

The transfer of metals from one surface to another at the atomic level has been observed and studied with each of these devices. The field ion microscope has been used to study polymer-metal interactions and Auger analysis to study the mechanism of polymer adhesion to metals. LEED and Auger analysis have identified surface segregation of alloying elements and indicated the influence of these elements in metallic adhesion. LEED and Auger analysis have assisted in adsorption studies in determining the structural arrangement and quantity of adsorbed species present making an understanding of the influence of these species on adhesion possible. In short these devices are assisting in the furtherance of our understanding of the fundamental mechanisms involved in the adhesion, friction, wear, and lubrication processes.

REFERENCES

1. H. Krupp: Adv. Colloid Interface Sci., 1 (1969), p. 264.

2. F. P. Bowden and D. Tabor: The Friction and Lubrication of Solids, Vols. I and II, Clarendon Press, Oxford, 1950.

3. D. H. Buckley: Friction, Wear, and Lubrication in Vacuum, NASA SP-277, 1971.

4. C. Davisson and L. H. Germer: Phys. Rev., 1927, vol. 30, p. 705.

5. H. E. Farnsworth: Phys. Rev., 1936, vol. 49, p. 605.

6. L. H. Germer and J. W. May: Surf. Sci., 1966, vol. 4, pp. 452-470.

7. R. M. Stern: Appl. Phys. Lett., 1964, vol. 5, pp. 218-220.

8. P. J. Estrup and E. G. McRae: Surf. Sci., 1971, vol. 25, pp. 1-52.

9. J. J. Lander: Phys. Rev., 1953, vol. 91, p. 1382.

10. L. A. Harris: J. Appl. Phys., 1968, vol. 39, pp. 1419-1427.

11. C. C. Chang: Surf. Sci., 1971, vol. 25, p. 53.

12. R. G. Musket and J. Ferrante: J. Vac. Sci. Tech., 1970, vol. 7, pp. 14-17.

13. E. W. Muller: Field Ion Microscopy, American Elsevier, 1969.

14. D. H. Buckley: J. Adhesion, 1969-1970, vol. 1-2, pp. 264-281.

15. D. H. Buckley: Wear, 20, 89 (1972).

16. E. Rabinowicz: Friction and Wear of Materials, John Wiley & Sons, Inc., New York, 1965.

17. J. Ferrante: Acta Met., 1971, vol. 19, pp. 743-748.

18. J. Ferrante: Scripta Met., 1971, vol. 5, p. 1129.

19. J. Ferrante: Thermal Effects in Equilibrium Surface Segregation In a Copper-10-Atomic-Percent-Aluminum Alloy Using Auger Electron Spectroscopy, NASA TM X-2543, Apr. 1972.

20. D. McLean: Grain Boundaries in Metals, Clarendon Press, Oxford, 1957.

21. M. D. Sanderson and J. C. Scully: Met. Trans., 1970, vol. 1, pp. 1273-1279.

22. D. H. Buckley and S. V. Pepper: Elemental Analysis of a Friction and Wear Surface During Sliding using Auger Spectroscopy, NASA TN D-6497, Sept. 1971.

23. S. V. Pepper and D. H. Buckley: Metallic Transfer Between Metals in Sliding Contact Examined by Auger Emission Spectroscopy, NASA TN D-6716, Mar. 1972.

24. C. S. Barrett: Structure of Metals, McGraw Hill Book Company, New York and London, 1943.

25. S. V. Pepper and D. H. Buckley: Adhesion and Transfer of PTFE to Metals Studied by Auger Emission Spectroscopy, NASA TM X-68076, June 1972.

26. K. R. Makinson and D. Tabor: Proc. Roy. Soc., Series A, 1964, vol. 281, p. 49.

27. E. W. Mueller and O. Nishikawa: in Spec. Tech. Publ. 431, ASTM, 1967, pp. 67-87.

28. W. A. Brainard and D. H. Buckley: Preliminary Studies by Field Ion Microscopy of Adhesion of Platinum and Gold to Tungsten and Iridium, NASA TN D-6492, Oct. 1971.

29. W. A. Brainard and D. H. Buckley: Adhesion of Polymers to Tungsten as Studied by Field Ion Microscopy, NASA TN D-6524, Oct. 1971.

30. A. G. Naumovets and A. G. Fedorus: Sov. Phys. Sol. State Phys., 1968, vol. 10, p. 627.

31. H. M. Montague-Pollock, T. N. Rhodin, and M. J. Southon: Surf. Sci., 1968, vol. 12, p. 1.

METAL	COHESIVE ENERGY KCAL/g ATOM	J/g ATOM	ATOMIC SIZE, Å (10^{-10} M)	VALENCY STATES	SOLUBILITY IN IRON, AT. %	ADHESION FORCE TO IRON,* DYNES (10^{-5} N)
IRON	99.4	40.5×10^4	2.86	2, 3	-----	>400
COBALT	101.7	42.6	2.50	2, 3	35	120
NICKEL	102.3	42.9	2.49	2, 3	9.5	160
COPPER	80.8	33.8	2.551	1, 2	< 25	130
SILVER	68.3	28.6	2.883	1	.13	60
GOLD	87.6	36.6	2.877	1	<1.5	50
PLATINUM	134.8	56.4	2.769	2, 4	20	100
ALUMINUM	76.9	32.3	2.80	3	22	250
LEAD	47.0	19.7	3.494	2, 4	INS	140
TANTALUM	186.7	78.1	2.94	5	.20	230

*APPLIED LOAD, 20 DYNES (20×10^{-5} N); TEMP, 20^0 C; AMBIENT PRESSURE, 10^{-10} TORR.

CS-64395

Table I. - Some properties of various metals and force of adhesion of these metals to iron.

E-7103

DISK	RIDER	TRANSFER OF METAL FROM RIDER TO DISK
TUNGSTEN	IRON	YES
	NICKEL	YES
	COBALT	YES
TANTALUM	IRON	NO
	NICKEL	NO
	COBALT	YES
MOLYBDENUM	IRON	NO
	NICKEL	NO
	COBALT	YES
NIOBIUM	IRON	NO
	NICKEL	NO
	COBALT	YES

CS-64377

Table II. - Metallic transfer for dissimilar metals in sliding contact.

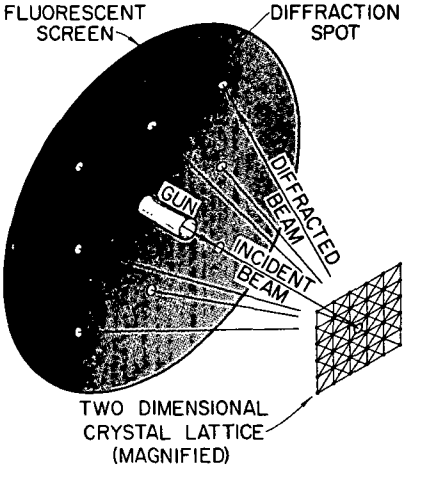

Figure 1. - Formation of diffraction pattern.

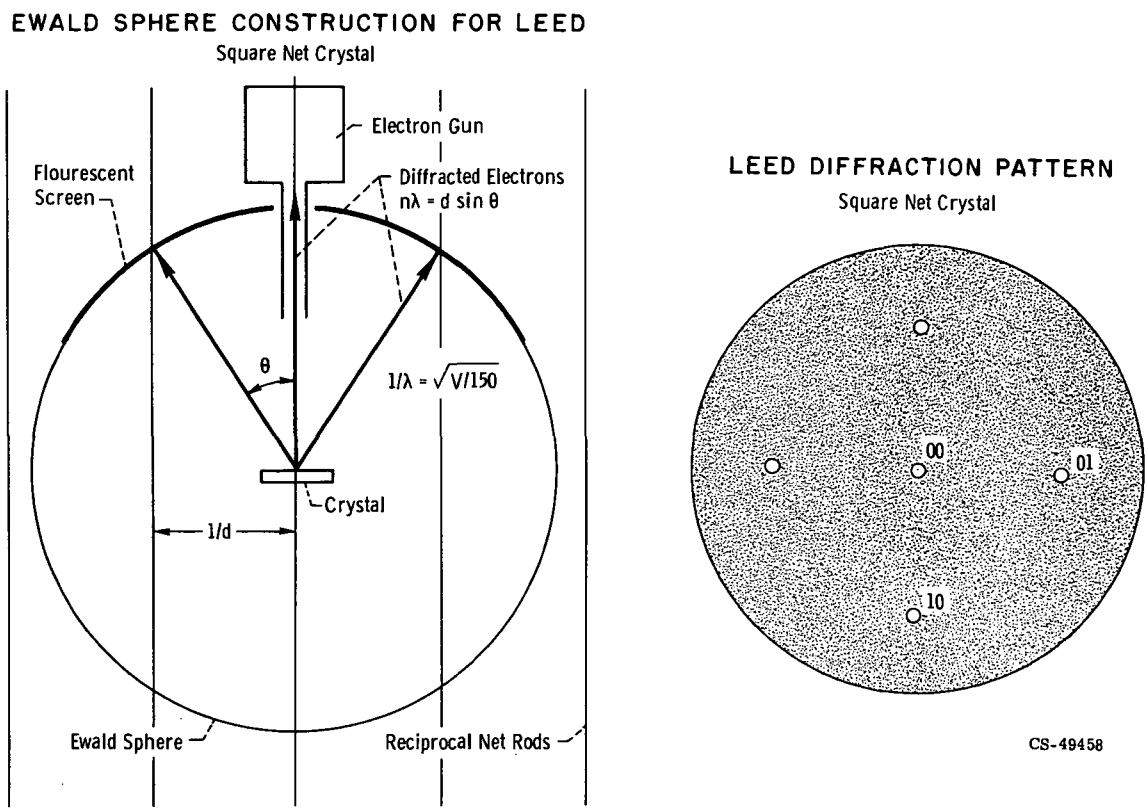

Figure 2. - Ewald construction for LEED with a square surface lattice.

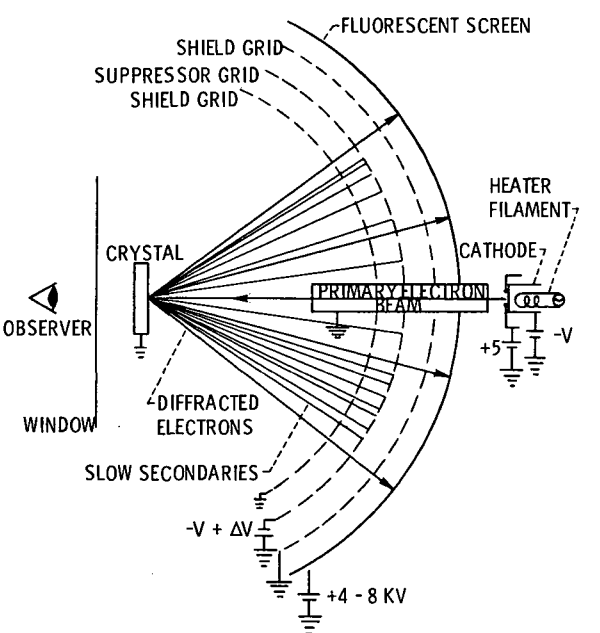

Figure 3. - LEED optics.

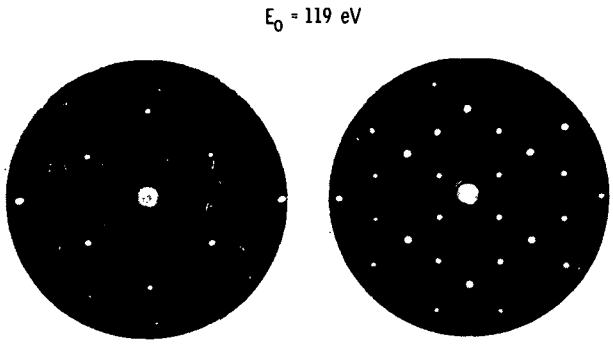

CS-50728

Figure 4. - LEED pattern for clean and oxidized W(110).

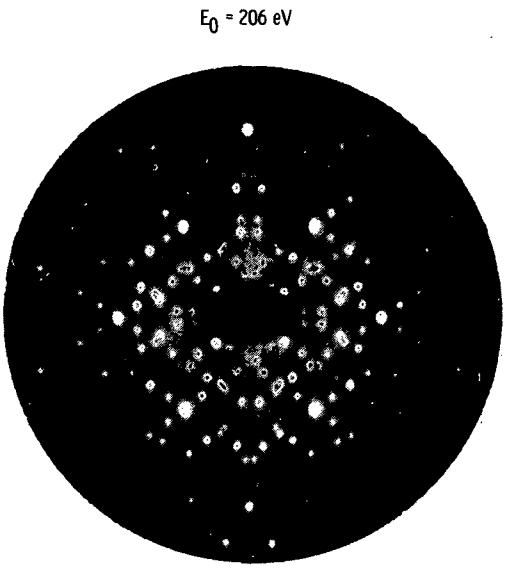

CS-49733

Figure 5. - LEED pattern of carbon contaminated W(110).

(R. M. Stern)

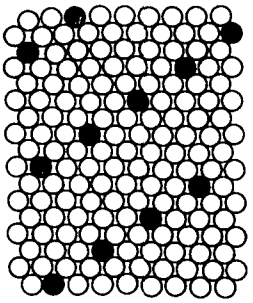

CS-49730

Figure 6. - Interpretation of surface structure in the direct lattice of carbon contaminated W(110).

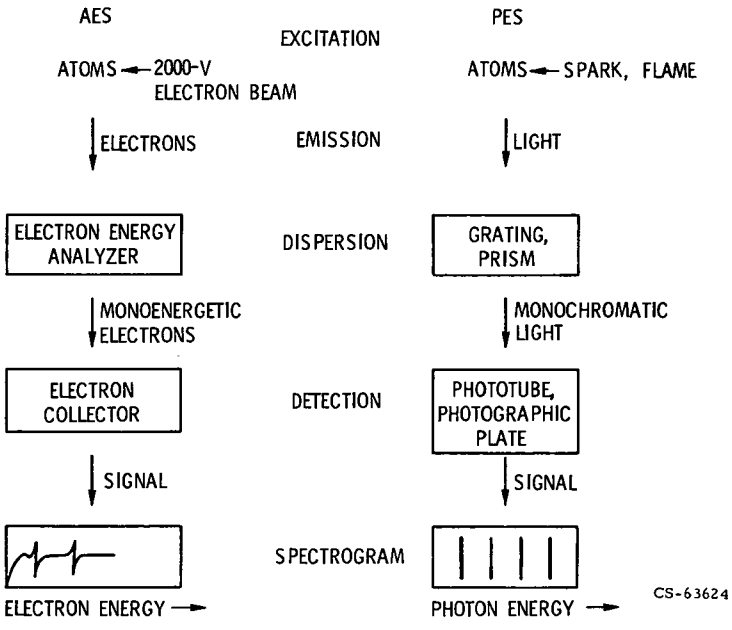

CS-63624

Figure 7. - A comparison of photon and Auger emission spectroscopy.

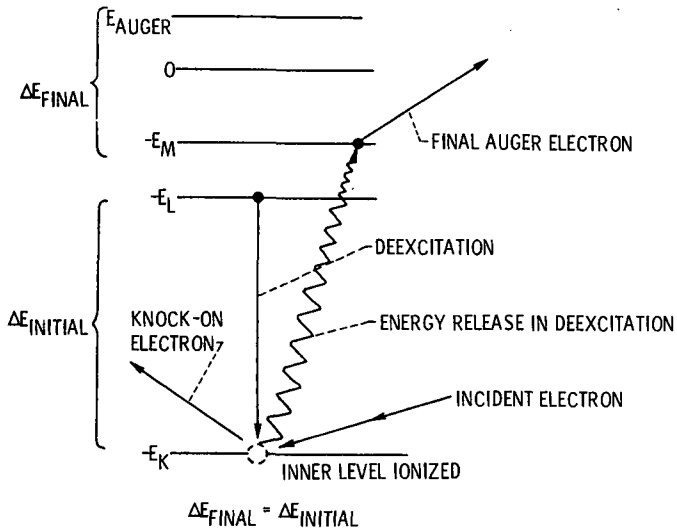

Figure 8. - Auger transition diagram for an atom.

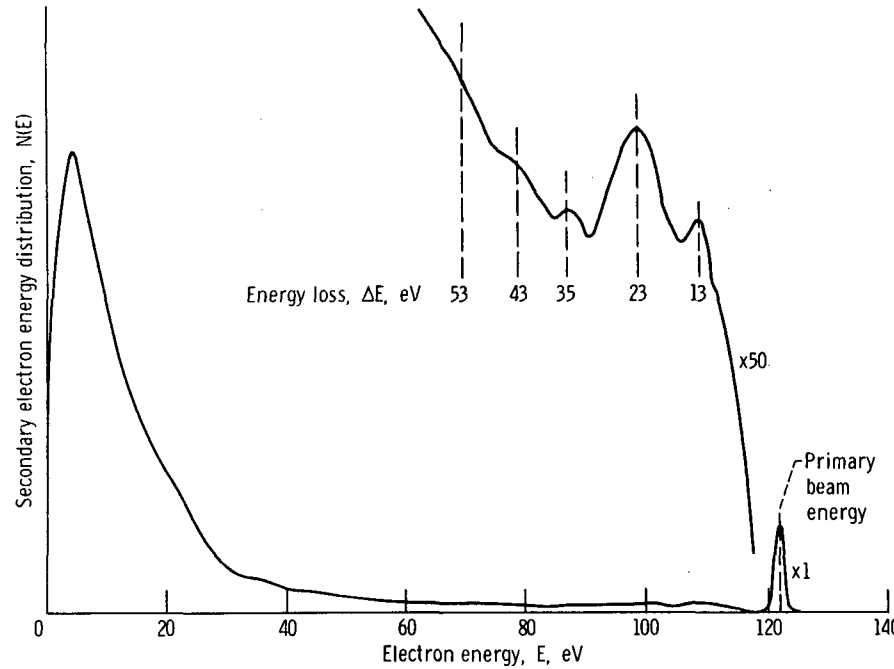

Figure 9. - Secondary electron energy distribution for 122 eV primary electrons on clean W(110).

CS-58860

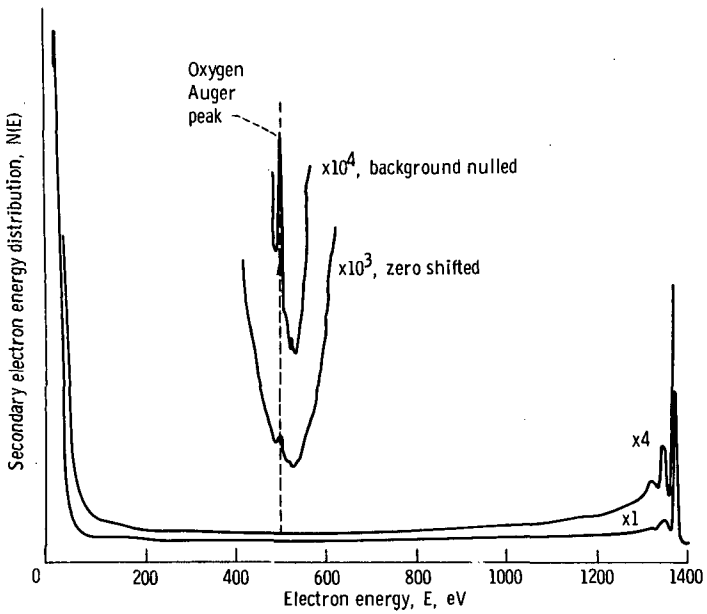

Figure 10. - Secondary electron energy distribution for 1365-eV electrons incident on W(110) exposed to 7.5 Langmuirs of oxygen, showing the oxygen Auger peak.

CS-58857

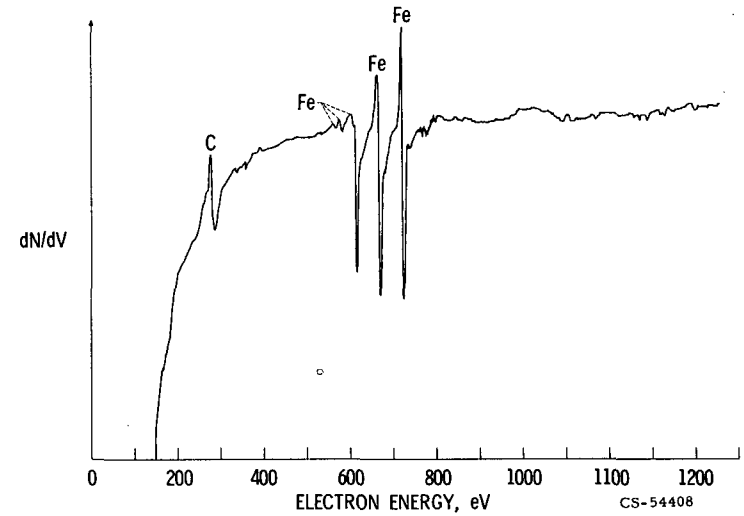

Figure 11. - Derivative of electron energy distribution for ethylene adsorbed on an Fe(001) surface.

SCHEMATIC OF EXPERIMENTAL ARRANGEMENT

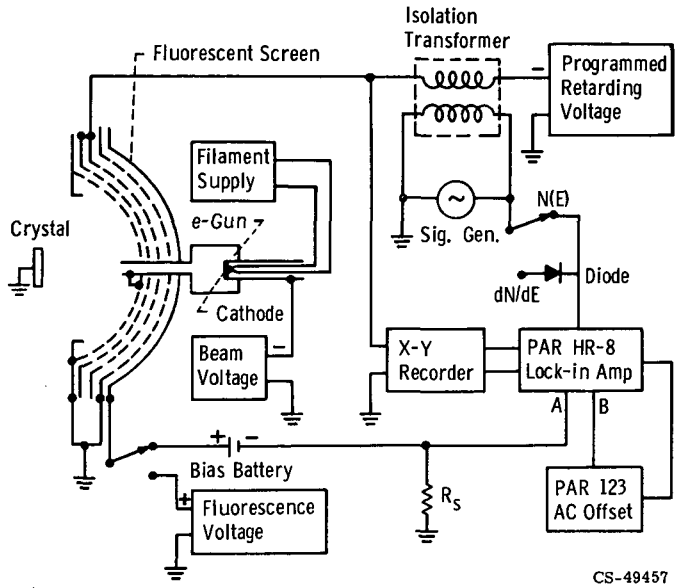

Figure 12. - Auger spectrometer using LEED optics.

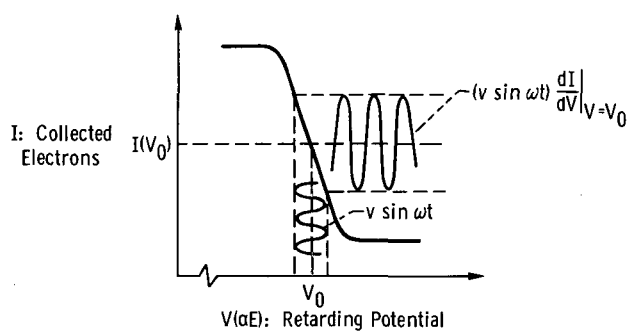

Taylor Series:

$$I(E) = I(E_0) + \left.\frac{dI}{dE}\right|_{E=E_0} (E - E_0) + \frac{1}{2!} \left.\frac{d^2I}{dE^2}\right|_{E=E_0} (E - E_0)^2 + \frac{1}{3!} \left.\frac{d^3I}{dE^3}\right|_{E=E_0} (E - E_0)^3 + \ldots$$

but, $E - E_0 = \varepsilon \sin \omega t$ and $N(E) = dI/dE$.

$$\therefore \quad I(E) = I(E_0) + \varepsilon N(E_0) \sin \omega t + \frac{\varepsilon^2}{4} \left.\frac{dN}{dE}\right|_{E=E_0} (1 - \cos 2\omega t) + \frac{\varepsilon^2}{24} \left.\frac{d^2N}{dE^2}\right|_{E=E_0} (3 \sin \omega t - \sin 3\omega t) + \ldots$$

CS-49459

Figure 13. - Principle of electronic differentiation for obtaining Auger spectrum.

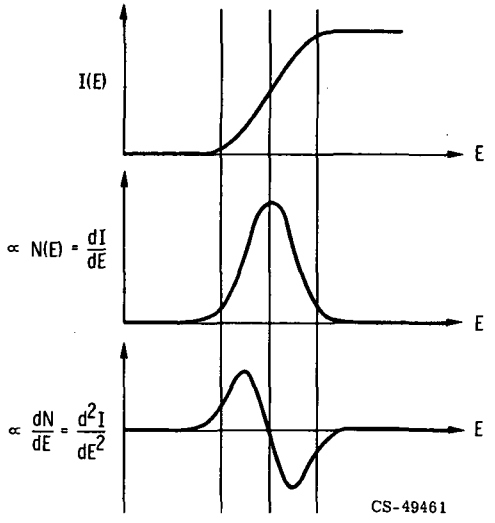

Figure 14. - Results of differentiation of various electron distributions.

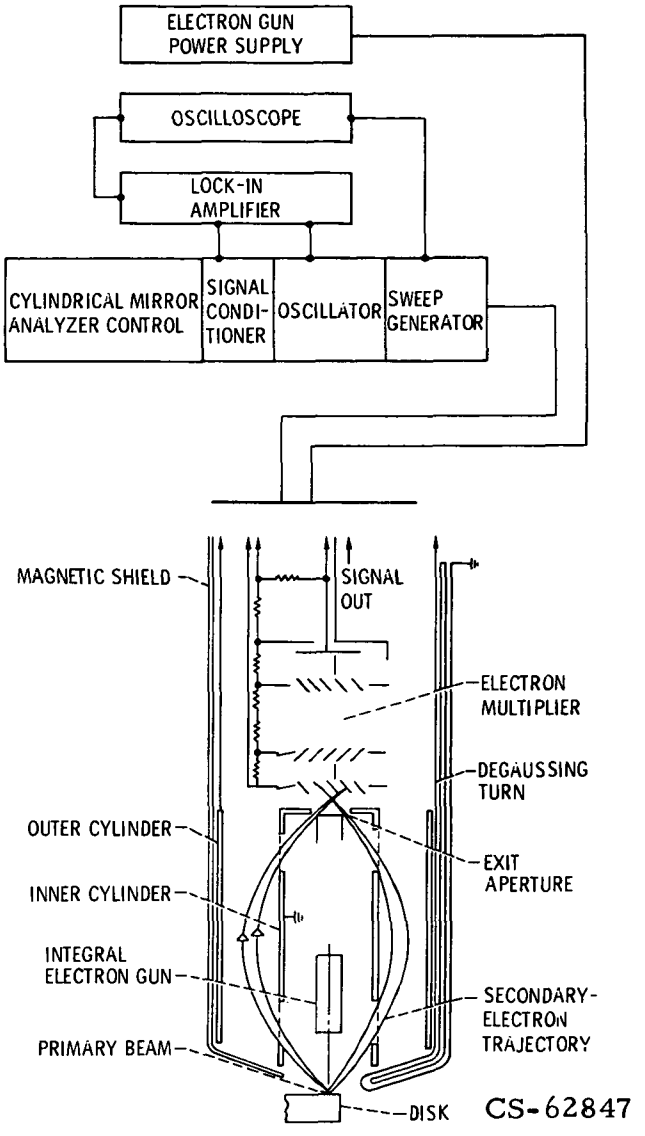

Figure 15. - Block diagram of Auger cylindrical mirror analyzer.

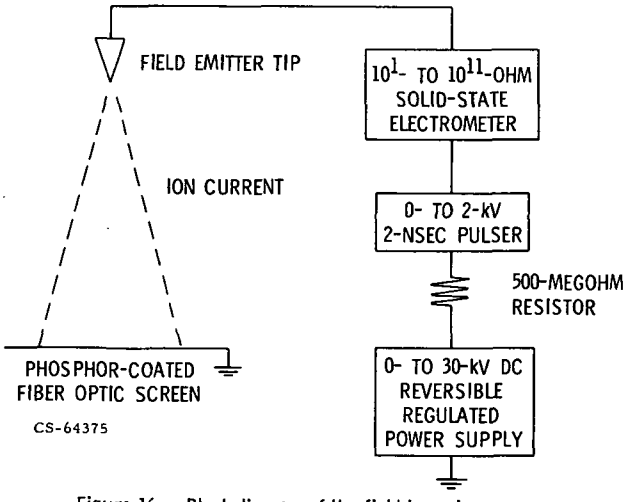

Figure 16. - Block diagram of the field ion microscope.

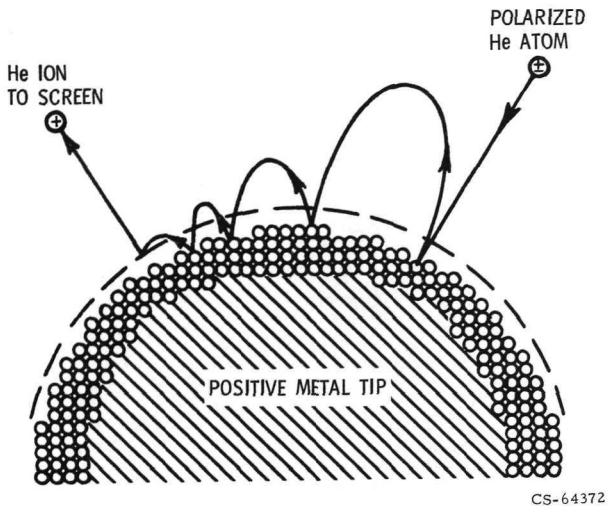

Figure 17. - The principle of field ion microscope image formation.

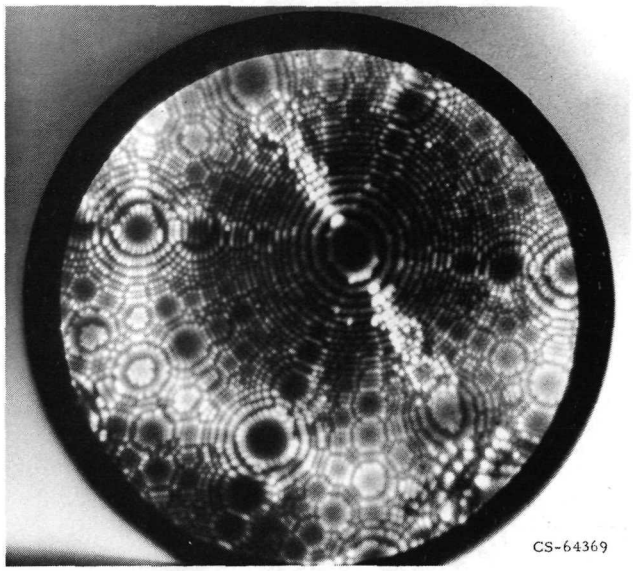

Figure 18. - Field ion microscope pattern of a clean tungsten tip oriented in the [110] direction.

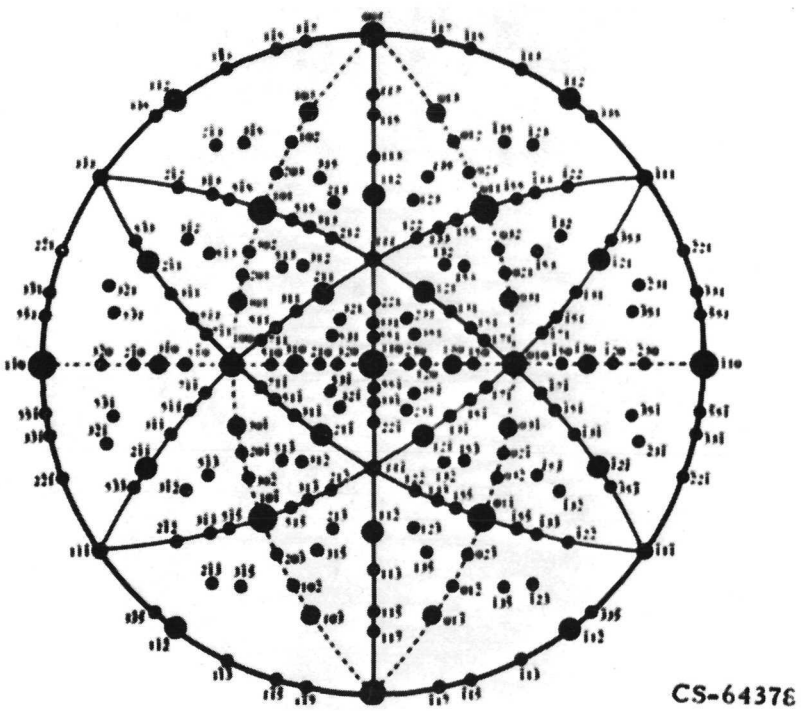

Figure 19. - Stereographic projection of a bcc lattice with the [110] direction normal to the page.

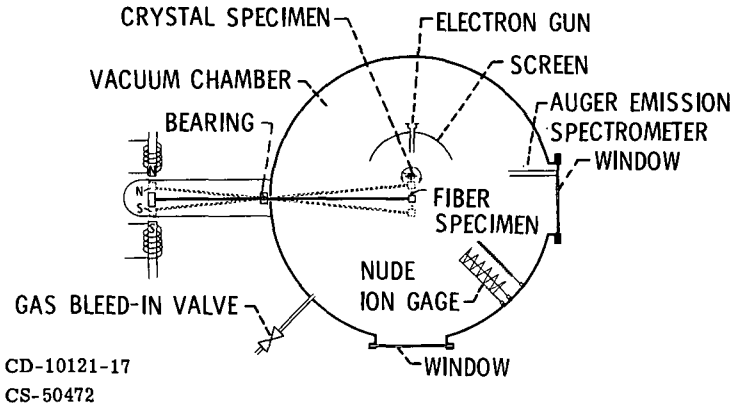

Figure 20. - LEED adhesion apparatus.

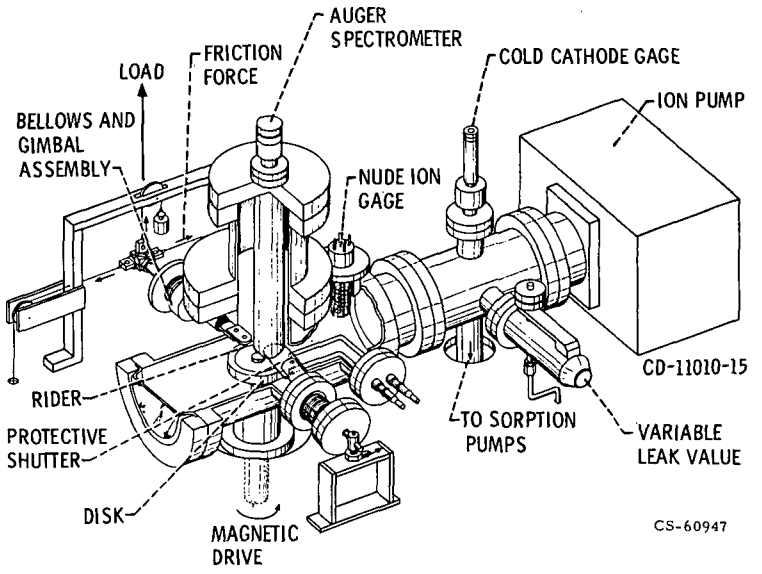

Figure 21. - Friction pin and disk apparatus equipped with Auger electron spectrometer.

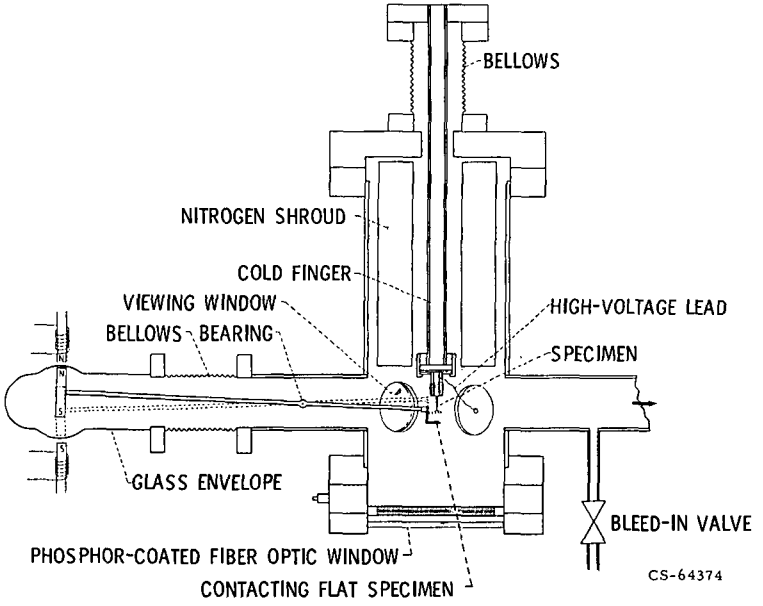

Figure 22. - Diagram of the FIM-adhesion apparatus.

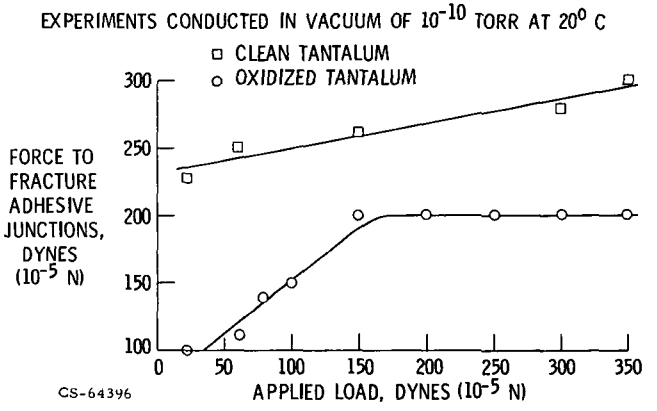

Figure 23. - Effects of oxygen adsorption on tantalum, on adhesion to a clean iron (011) surface.

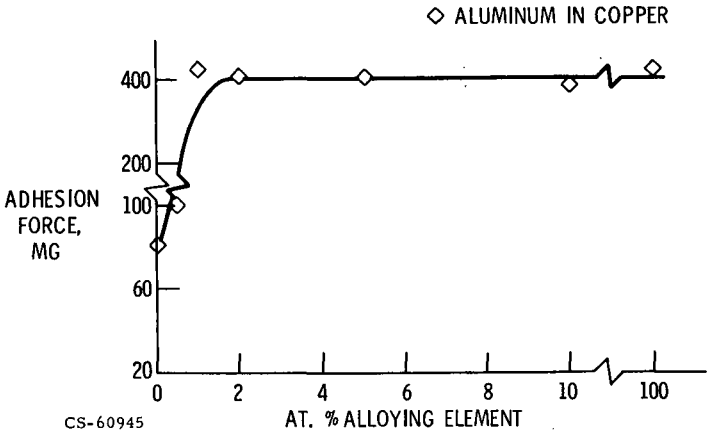

Figure 24. - Effects of alloying on adhesion of gold to single crystal copper-aluminum alloys oriented in the (111) direction.

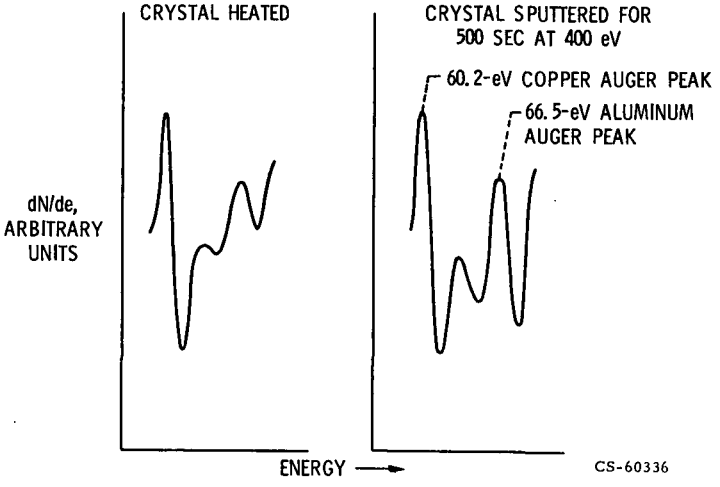

Figure 25. - Increase in aluminum surface concentration following sputtering, then annealing in a copper-10 percent aluminum alloy.

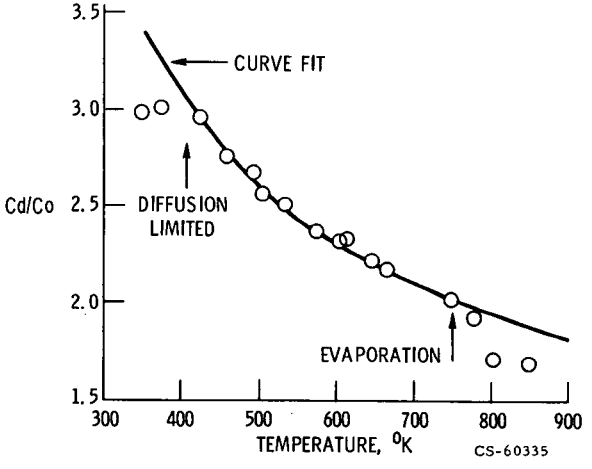

Figure 26. - Effect of temperature on the surface concentration of aluminum in a copper-10-a/o-aluminum alloy.

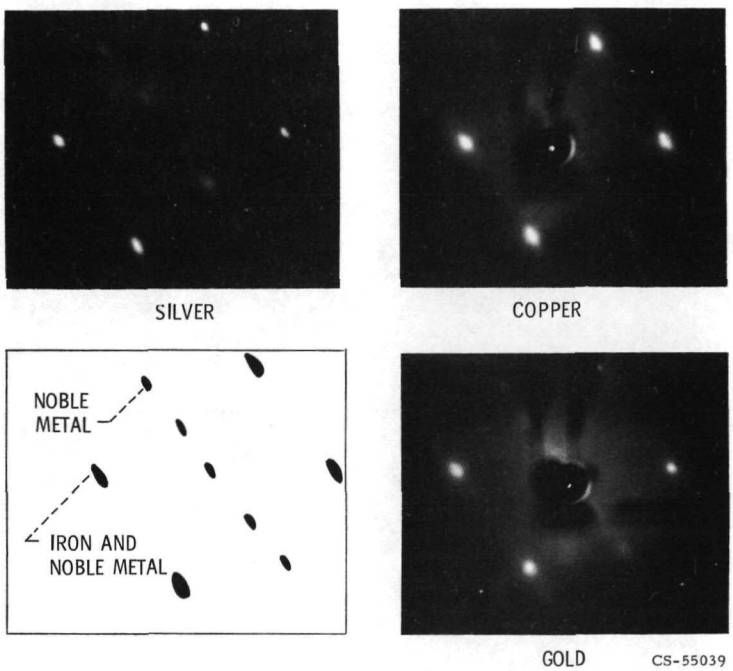

Figure 27. - LEED patterns resulting from the adhesion of (111) planes of copper, silver, or gold with the (110) surface of iron.

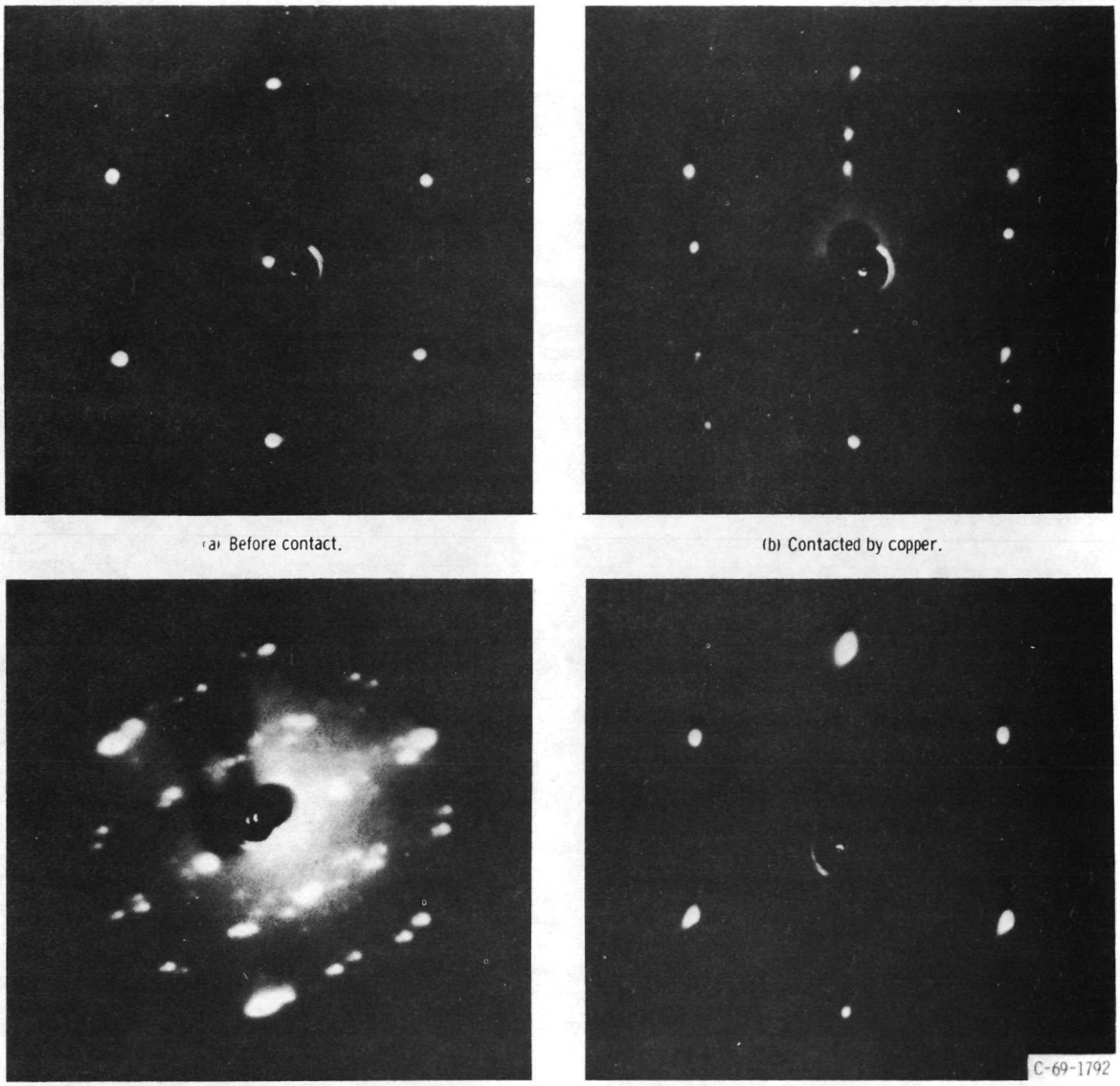

(a) Before contact.

(b) Contacted by copper.

(c) Contacted by lead.

(d) Contacted by platinum.

Figure 28. - LEED patterns resulting from the adhesion of the most densely packed planes of copper, lead, and platinum to a nickel (111) surface.

C-69-1792
CS-64551

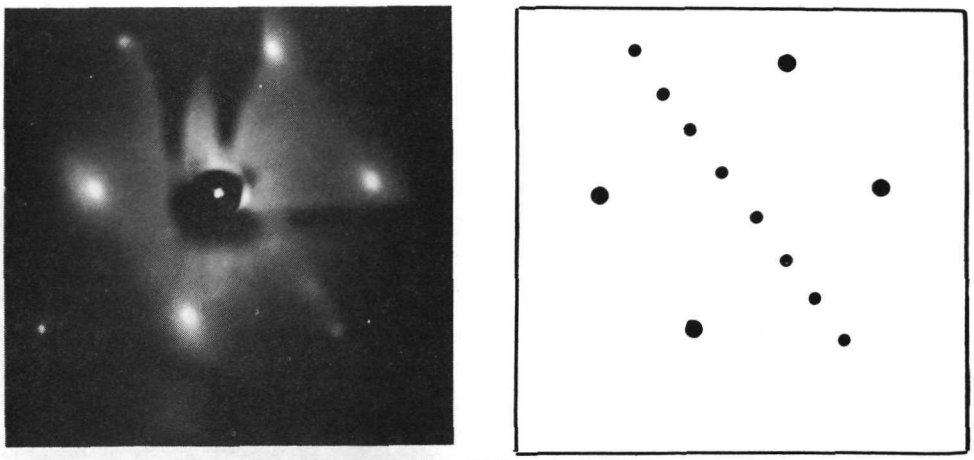

NICKEL WITH OXIDE PRESENT

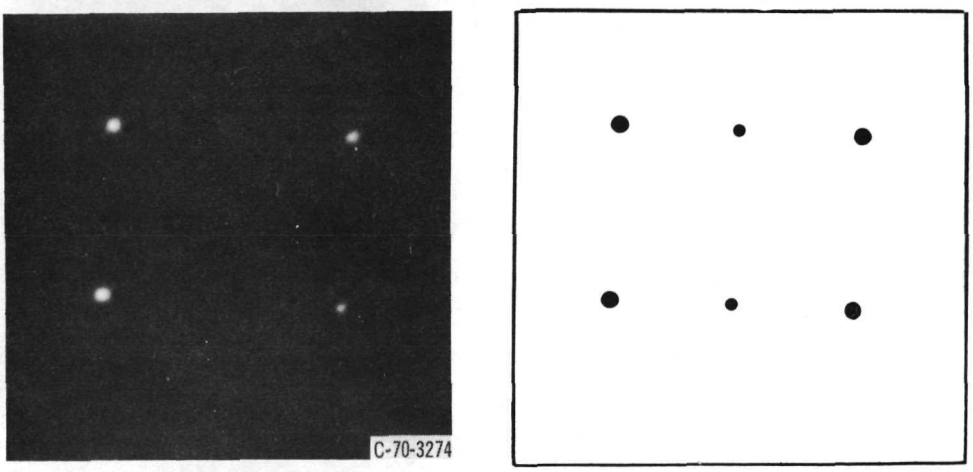

TANTALUM WITH OXIDE PRESENT

CS-64394

Figure 29. - Adhesion of oxidized tantalum and nickel to an iron (110) surface.

20 CM/MIN; 500 g; 23^{0} C

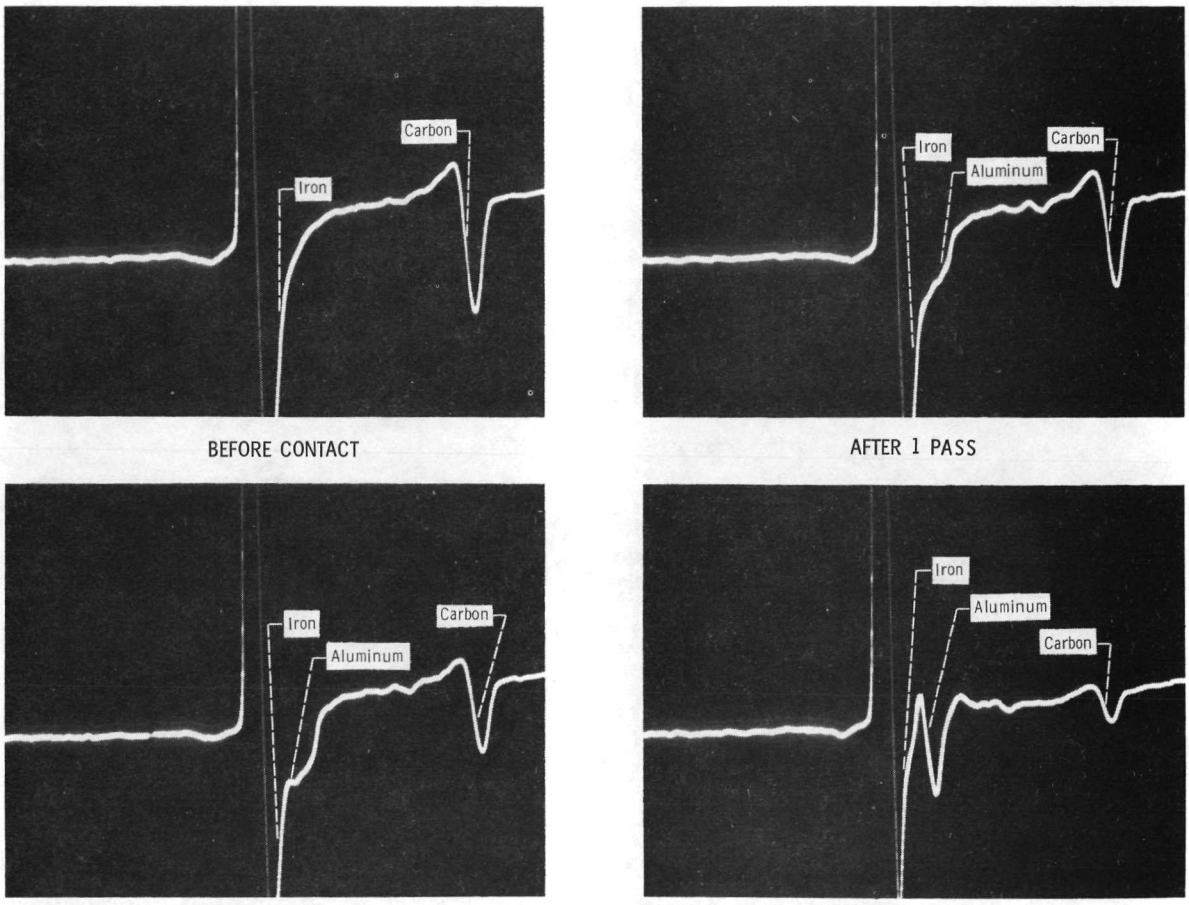

BEFORE CONTACT

AFTER 1 PASS

AFTER 5 PASSES

AFTER 20 PASSES CS-62854

Figure 30. - Auger analysis of a steel disk before and after contact with an aluminum rider.

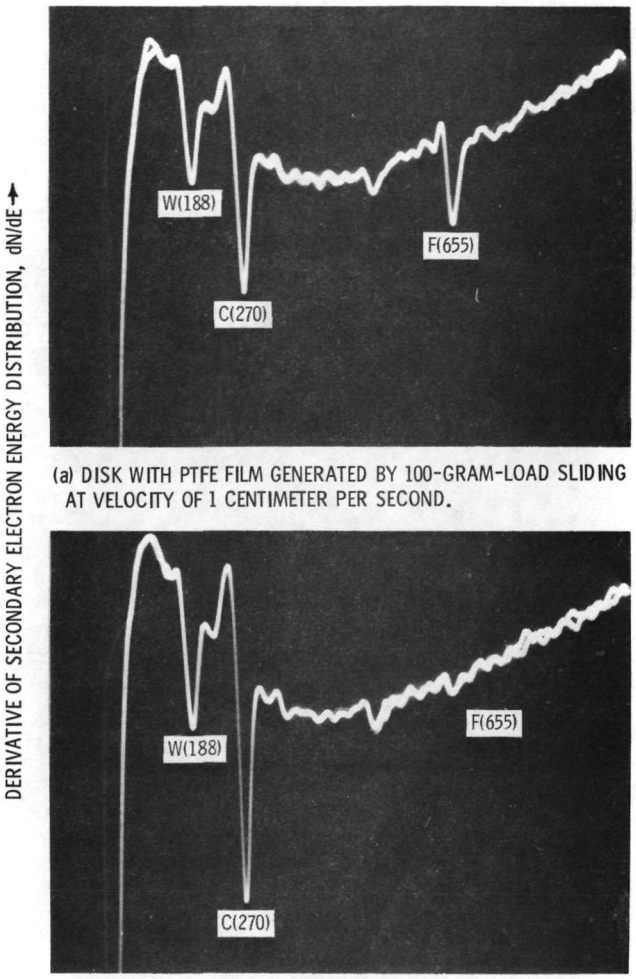

(a) DISK WITH PTFE FILM GENERATED BY 100-GRAM-LOAD SLIDING AT VELOCITY OF 1 CENTIMETER PER SECOND.

(b) SAME SPOT ON DISK AS IN (a) AFTER 1-MINUTE TIME INTERVAL; 70-MICROAMPERE BEAM CURRENT.

Figure 31. - Detection of transfer of PTFE to a tungsten disk using AES, and detection of electron impact desorption of the fluorine.

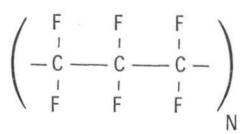

Figure 32. - Chemical structure of a PTFE chain.

CS-63740

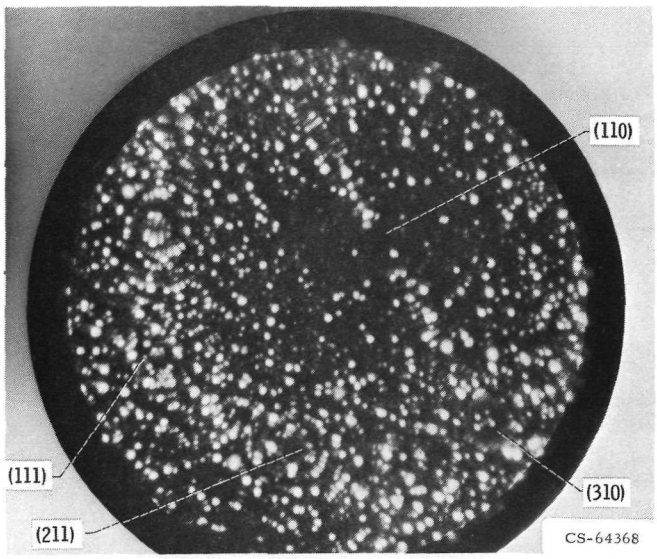

Figure 33. - Results of contact of a tungsten FIM tip with platinum.

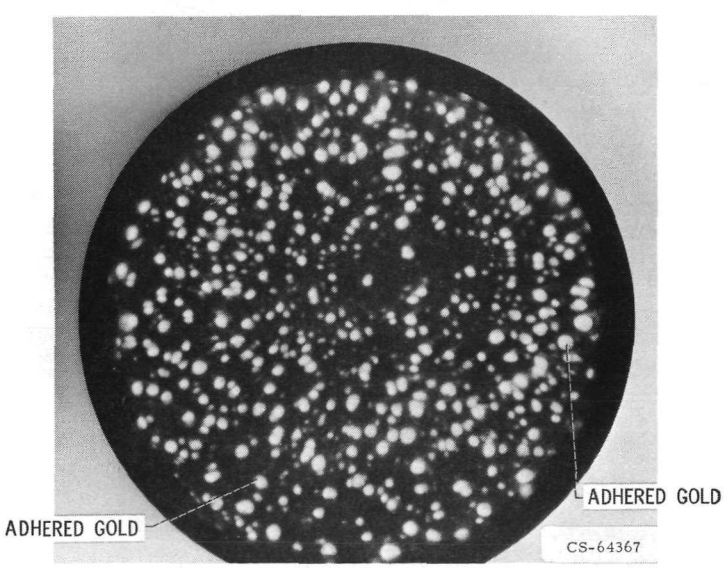

Figure 34. - Results of contact of gold with a tungsten FIM tip.

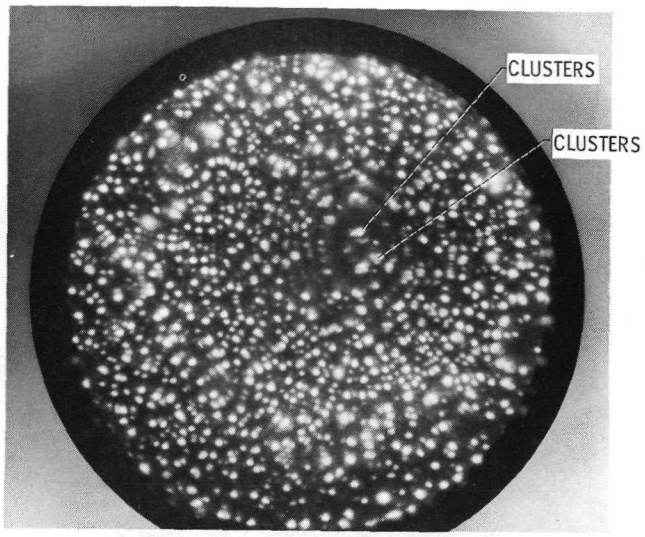

CS-64476

Figure 35. - Figure 34 with increased imaging voltage.

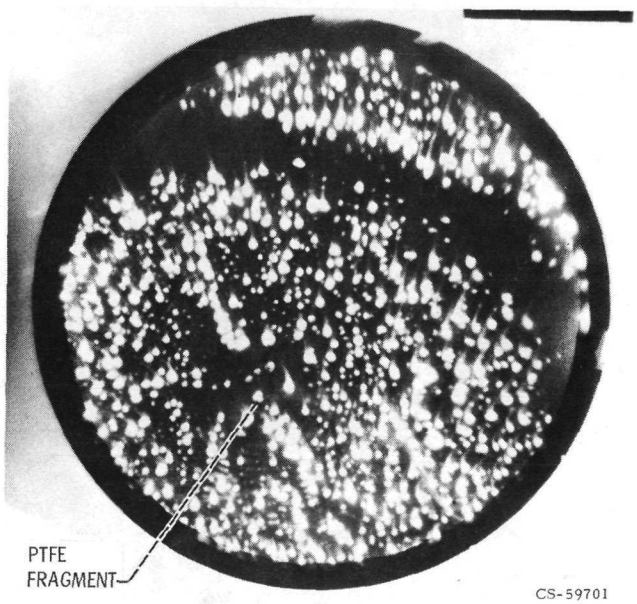

CS-59701

(a) FIM PATTERN.

Figure 36. - Results of contact of a tungsten FIM tip with PTFE.

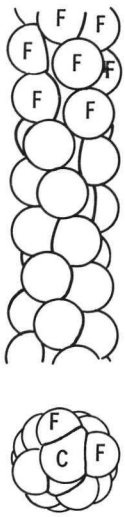

CS-64376

(b) END AND SIDE VIEW OF A PTFE CHAIN.

Figure 36. - Concluded.

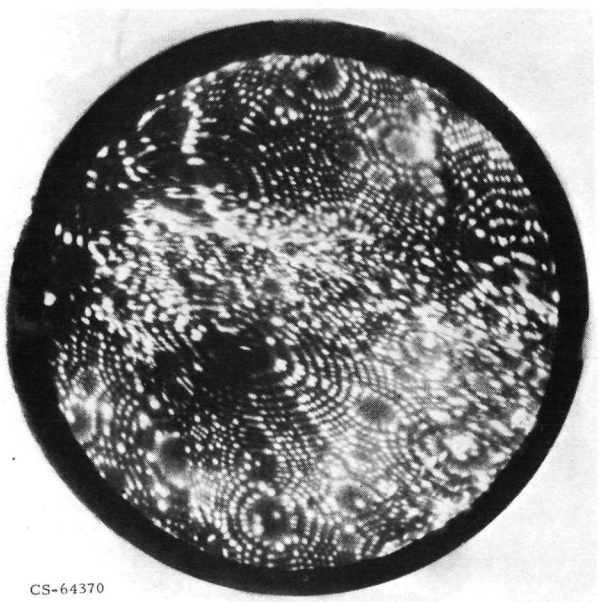

CS-64370

Figure 37. - Deformation of a tungsten tip after contact with PTFE at a heavy load.